

Enhancement in physical properties of Pb-Based Perovskite Oxides ($PbGeO_3$): Ab initio Calculation

M. Agouri¹, A. Waqdim¹, A. Abbassi^{1,*}, M. Ouali¹, S. Taj¹, B. Manaut^{1,†}, M. Driouich¹

¹ *Laboratory of Research in Physics and Engineering Sciences,
Sultan Moulay Slimane University, Polydisciplinary Faculty, Beni Mellal, 23000, Morocco.*

February 1, 2023

Abstract

In the present paper, the electronic, structural, thermodynamic, and elastic properties of cubic $PbGeO_3$ perovskite oxide are presented and computed using the WIEN2k code. The structural properties have been evaluated and they are in good agreement with the theoretical and experimental data. A phonon dispersion is made and it reveals that the cubic $PbGeO_3$ perovskite is dynamically stable. In addition, the electronic properties of $PbGeO_3$ shows an opening gap energy, meaning a semiconductor behavior with an indirect band gap equal to 1.67 eV. Moreover, the obtained elastic constants of cubic $PbGeO_3$ satisfy Born's mechanical stability criteria, and this indicates that our compound behaves as a stable ductile material. The temperature-pressure effects on thermodynamic parameters are investigated using the Gibbs2 package. Finally, based on the obtained results about the cubic $PbGeO_3$ perovskite properties, we assume that this compound will have potential applications.

Keywords: DFT, Elastic, Thermodynamic, Perovskite, WIEN2K, mBJ.

*Corresponding author, E-mail: abbassi.abder@gmail.com

†Corresponding author, E-mail: b.manaut@usms.ma

1. Introduction

Since the discovery of $CaTiO_3$ [1], the perovskite oxides family has been a major subject of interest, and this is mainly due to its multi-functional character [2,3]. It has received great attention for its exploitation in many applications such as solar cells [4], spintronic and optoelectronic [5,6]. The exploitation of these materials mainly depends on their flexible structure, variable formula, and also their various properties [7,8]. Consequently, a lot of experimental and theoretical studies have proved that the perovskite oxides family has unique physical properties like photoelectric [9], magnetic [10], ferroelectric [11],... etc.

Pb-based perovskite oxides have long been investigated for their rich and interesting properties. They are considered proper candidates in energy conversion such as in piezoelectric and ferroelectric devices [12]. Recently, several experimental and theoretical studies have been interested on Lead-based perovskite oxides. The unit cell compounds of $PbXO_3$ ($X = Ti, V$) were synthesized, and their crystal structures are determined using Neutron and X-ray diffraction [13,14]. In addition, these compounds have largely been used in ferroelectric and optical sensors [15,16]. The $PbZr_xTi_{1-x}O_3$ ($x = 0, 0.4, 0.6, 1$) were prepared and investigated, proving the exploitation of these compounds in optical applications [17]. The structural, magnetic, and electronic properties of tetragonal structures ($Pbmm$ and $P4/mmm$) of $PbMnO_3$ were calculated theoretically using the density functional theory (DFT) approach [18]. Besides, J.B. Goodenough *et al.*, showed in [19] the varied roles of Pb in transition-metal $PbTMO_3$ ($TM = V, Mn, Ni, Mn, Ti, Fe, Ru$) perovskites.

Due to its excellent and unique physical properties, Cubic $PbGeO_3$ perovskite oxide have received more attention in both experimental and theoretical physics. In addition, the $PbGeO_3$ perovskite crystallizes in cubic structure which is reported in experimental and theoretical works [20]. Using X-ray photoelectron spectroscopy, they have calculated the binding energy of the $PbGeO_3$ and $Pb_5Ge_3O_{11}$ phases and showed their optical transmission characteristics [11]. Other researchers showed that $PbGeO_3$ is considered an interesting choice for lithium batteries [21,22]. Theoretically, optoelectronic and thermoelectric properties of cubic $PbGeO_3$ were evaluated within the DFT approach [23].

In this paper, we investigate the electronic, structural, thermodynamic and elastic properties of cubic $PbGeO_3$ perovskite oxide using Full Potential Linearised Augmented Plane Wave (FP-LAPW) method within the DFT approach. Our report is structured as follows: We start with computational procedures, and then we analyze and discuss the obtained results about the studied physical

properties of $PbGeO_3$ perovskite. Finally, a conclusion of the main results is given in the last section.

2. Computational details

In this paper, we investigate the physical properties of cubic $PbGeO_3$ perovskite oxide by using the FP-LAPW method within DFT approach [24] as implemented in the WIEN2k code [25]. Based on the Perdew-Burke-Ernzerhof approximation (PBE-GGA) [26] and modified Becke-Johnson (mBJ) exchange potential [27], we have studied the structural and electronic properties of the $PbGeO_3$ perovskite oxide. The elastic parameters have been determined using ElaStic-1.1 package [28]. The separation energy between core and valence electrons is -10.0 Ry . The number of plane waves is limited by $R_{MT} \times K_{max} = 8$. The l_{max} parameter is taken to be 10 and the Fourier expanded charge density is $G_{max} = 12$. The integration of first Brillouin zone is performed with $(6 \times 6 \times 6)$ k-points grid in reciprocal space. The crystal structure is designed using VESTA program [29].

The thermodynamic parameters of the cubic $PbGeO_3$ are determined by using the quasi-harmonic Debye model [30, 31]. The non-equilibrium Gibbs function $G^*(P, V, T)$ is defined by the following equation :

$$G^*(P, V, T) = E(V) + PV + H_{vibration}[\Theta_D(V), T], \quad (1)$$

where PV represents the constant hydrostatic pressure condition and $E(V)$ is the equilibrium energy per unit cell.

The $H_{vibration}[\Theta_D(V), T]$ denotes the vibrational term, which can be written as:

$$H_{vibration}(\Theta_D(V), T) = mK_B T \left\{ \frac{9\Theta_D}{8T} + 3 \ln \left(1 - e^{-\Theta_D/T} \right) - D \left(\frac{\Theta_D}{T} \right) \right\}, \quad (2)$$

where m represents the number of atoms per formula and $D \left(\frac{\Theta_D}{T} \right)$ is the Debye integral.

The Debye temperature Θ_D is expressed as :

$$\Theta_D = \frac{\hbar}{K_B} \left(6\pi^2 V^{1/2} m \right)^{1/3} f(\sigma) \sqrt{\frac{B_s}{M}}, \quad (3)$$

where M stands for the molecular mass per unit cell.

The adiabatic bulk modulus B_T is approximately defined as the static compressibility :

$$B_T \approx B(V) = V \frac{d^2 E(V)}{dV^2}. \quad (4)$$

The $G^*(P, V, T)$ function is minimized with respect to the volume V as:

$$\left[\frac{dG^*(P, V, T)}{dV} \right]_{P, T} = 0. \quad (5)$$

By solving the equation (5), we find the thermal equation of states $V(P, T)$.

The thermal expansion α , bulk modulus B and the heat capacity (at volume constant) C_V are successively given by the following equations [30]:

$$\alpha = \frac{\gamma C_V}{B_T V}, \quad (6)$$

$$B_T = V \left(\frac{d^2 G^*(P, V, T)}{d^2 V} \right)_{P, T}, \quad (7)$$

$$C_V = 3mk \left[4D \left(\frac{\Theta}{T} \right) - \frac{3\Theta/T}{e^{\Theta/T} - 1} \right]. \quad (8)$$

3. Results and discussions

3.1. Structure and stability

Perovskite oxide $PbGeO_3$ was first optimized based on the experimental lattice parameter. $PbGeO_3$ has an ideal cubic phase with a space group $Pm\bar{3}m$. The atomic coordinates of the primitive cell of cubic $PbGeO_3$ are defined as Pb : $(0, 0, 0)$, Ge : $(1/2, 1/2, 1/2)$ and O : $(0, 1/2, 1/2)$. Figure 1 shows the variation of the total energy as a function of the unit cell volume in addition to the flexible structure of cubic $PbGeO_3$.

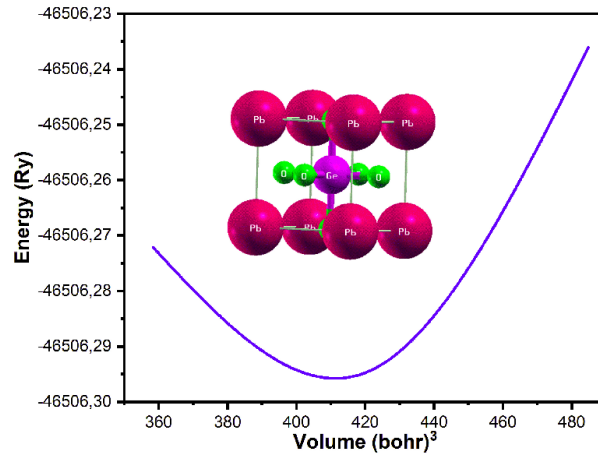


Figure 1: The crystal structure and the optimization plot of $PbGeO_3$.

The calculated values of lattice constant (a) and bulk modulus (B) of our compound are summarized in table 1. We notice that the obtained results are in good agreement with the theoretical and experimental works [20, 23].

Compound	$a(\text{\AA})$	$B(\text{GPa})$	Methods
$PbGeO_3$	3.8984	152.5279	Our work
	3.9680		Exp [20]
	3.8320, 3.8420, 3.9002, 3.8404, 3.8536, 3.8150.	198, 157.8647, 180.7519, 181.9745, 201.1913.	Theory [20, 23]

Table 1: Calculated lattice constant (a) and Bulk modulus (B) of $PbGeO_3$ compound.

In order to examine the dynamic stability of cubic $PbGeO_3$, we have calculated the phonon dispersion using the supercell method within phonopy code [32]. Figure 2 presents the phonon dispersion of our material $PbGeO_3$. According to this figure, the phonon dispersion curve of our compound shows positive frequencies along the high symmetry directions, indicating the dynamic stability of the cubic $PbGeO_3$ phase.

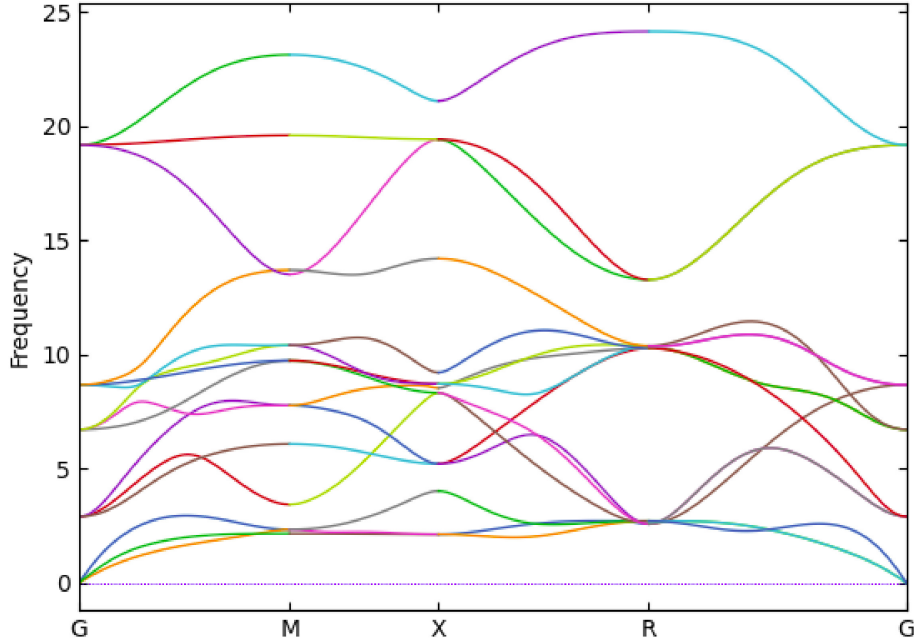


Figure 2: Phonon dispersion curve of $PbGeO_3$.

4. Electronic properties

Regarding the electronic properties of cubic $PbGeO_3$, we have investigated the band structure, partial and total density of state using PBE + TB-mBJ exchange-correlation potential. We mention that,

the mBJ approach gives a large band gap energy, and it solves the problem of underestimation band gap energy [27].

Figure 3 shows the obtained electronic band structure of $PbGeO_3$ along the high symmetry directions using the mBJ approach. We can see from this figure that $PbGeO_3$ shows a semiconductor behavior. In addition, we note that the valence band maximum (VBM) and the conduction band minimum (CBM) are placed, respectively, at X and Γ points. This means that $PbGeO_3$ has an indirect band gap equal to 1.67 eV (Γ - X). Moreover, our result is consistent with other theoretical calculation (A.Day *et al.* [23]).

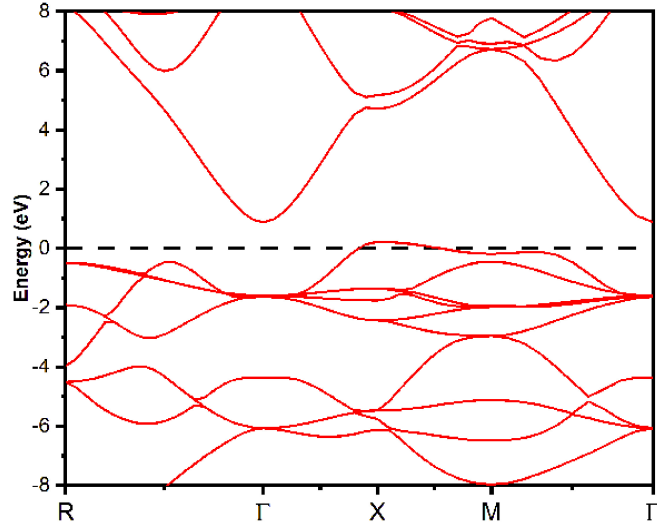


Figure 3: Band structure of $PbGeO_3$ using mBJ approach.

For a better illustration of the contribution of different band energies in the band structure, we have calculated the partial and total density of states as presented in figure 4. We note that the lower region of the valence band consists of all orbitals such as $s - Pb$, $sp - Ge$ and p of Oxygen with hybridization between Pb and Oxygen in TDOS. Near the Fermi level, the p -Oxygen is mixed with $s - Pb$ which represents a strong hybridization of p and s of Oxygen and Lead, respectively. The gap energy is clearly shown due to the contribution of the $s - Ge$ and p orbitals of Oxygen. For the conduction band (CB), a large dispersion of s orbital of Ge is observed, and it forms a covalent chemical bond with the p orbital of oxygen. Similar results are shown in the case of $SrGeO_3$ [33]. Besides, we observe a hybrid state between the p orbitals of Pb and Oxygen around 5 eV.

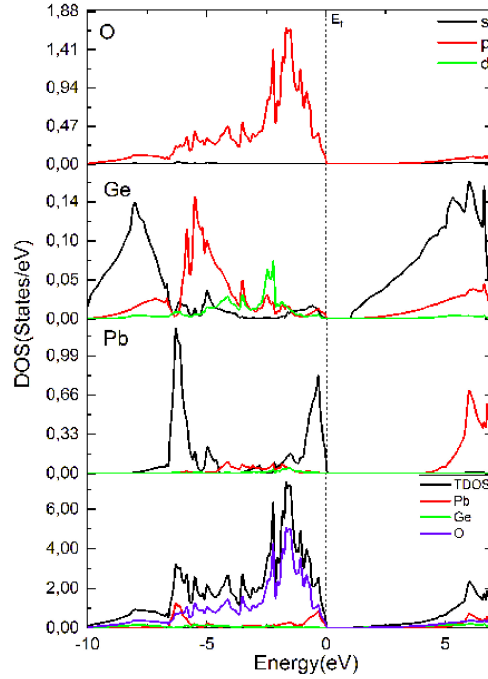


Figure 4: The partial and total density of the states of $PbGeO_3$ using the mBJ approach.

4.1. Elastic properties

Elastic constants play a significant role in material engineering as it provides important information about the ductility, brittleness, stillness, and also the mechanical stability of materials [34]. The elastic properties of cubic $PbGeO_3$ are investigated using the ElaStic1-1 package [28]. $PbGeO_3$ is a cubic crystalline structure, which has three independent elastic constants (C_{11} , C_{12} and C_{44}). Table 2 shows the calculated elastic constants of our compound using the modified Becke Johnson (mBJ) approximation. We note that C_{11} represents the longitudinal distortion (compression) and describes the hardness of the material, C_{12} is based on the transverse distortion (compression) and C_{44} represents the resistance to shear deformation, which is based on the shear modulus [34].

The mechanical stability is verified using Born's criteria that are given by [35]:

$$\begin{cases} C_{11} - C_{12} > 0, \\ C_{44} > 0, \\ C_{11} + 2C_{12} > 0. \end{cases} \quad (9)$$

From Table 2, the calculated elastic constants respect Born's criteria, and this clearly means that cubic $PbGeO_3$ is mechanically stable. From table 2, one can see that the longitudinal distortion

value is higher than C_{44} value, meaning a weak resistance to the shear modulus compared to the longitudinal distortion [36].

Elastic Coefficients			
Coefficient	C_{11}	C_{12}	C_{44}
PbGeO ₃	153.4	141.1	115.5

Table 2: The obtained elastic constants of the $PbGeO_3$ compound.

Based on elastic constant $C_{\alpha\beta}$, The mechanical constants such as shear modulus (G), bulk modulus (B), Cauchy pressure (C''), Pugh's ratio (B/G), Poisson's ratio (ν), anisotropy (A) are calculated through the VRH (Voigt-Reuss-Hill) approximation by using the following formulas [37, 38]:

$$B = \frac{2C_{12} + C_{11}}{3}, \quad G = \frac{G_R + G_V}{2}, \quad Y = \frac{9BG}{3B + G}, \quad \nu = \frac{3B - 2G}{2(G + 3B)}, \quad (10)$$

where G_R and G_V are successively the shear modulus of Reuss and Voigt approaches such that:

$$G_V = \frac{C_{11} + 3C_{44} - C_{12}}{5}, \quad G_R = \frac{5C_{44}(C_{11} - C_{12})}{3(C_{11} + C_{12} + 4C_{44})}. \quad (11)$$

The obtained results of mechanical parameters are listed in table 3. The bulk and shear modulus can be used to measure the rigidity of materials [37]. The calculated G and B values are 43.03 GPa and 145.18 GPa , respectively. We notice that the B value found from elastic constants is nearer to that obtained by fitting the Birch-Murnaghan equation of state. This comparison ensures that our computed elastic constants are correct. In addition, Young's modulus Y also deals with the hardness or stillness of materials [39]. The obtained value of Y is equal to 117.49 GPa , which is important as it is greater than 100. Therefore, we assume that $PbGeO_3$ behaves as a hard material. Anisotropy (A) is also an important parameter in industrial science for detecting micro-cracks in materials [40]. From table 3 the calculated value of A is 0.6, meaning that $PbGeO_3$ shows an anisotropy aspect.

The Poisson's ratio (ν), Cauchy pressure (C'') and Pugh's ratio (B/G) reveal the ductile or brittle aspect of materials. It is well known that the critical value of Pugh's ratio (B/G) which separates the ductile/brittle aspect is found to be 1.75. Consequently, a material will show a ductile aspect for values of B/G higher than 1.75, while it shows a brittle nature for values of B/G less than this critical value [41]. Another index of brittleness/ductility is the Cauchy pressure (C''). The positive and negative values of C'' are, respectively, related to the ductility and brittleness nature [42]. The parameter of Poisson's ratio (ν) is also a significant factor to distinguish the ductility/brittleness of materials with its critical value which is 0.26. The material will be ductile (brittle) when the Poisson's ratio is higher (less) than 0.26 [43]. Based on these roles and the obtained results, we conclude that $PbGeO_3$ shows a ductility aspect.

Mechanical Constants							
Constant	$B(\text{GPa})$	$G(\text{GPa})$	B/G	$Y(\text{GPa})$	$C''(\text{GPa})$	ν	A
PbGeO_3	145.18	43.03	3.37	117.49	25.6	0.37	0.67

Table 3: The obtained values of shear modulus G , bulk modulus B , Pugh's ratio B/G , Young's modulus Y , Poisson's ratio ν , Cauchy pressure C'' and elastic anisotropic factor A of PbGeO_3 compound.

4.2. Thermodynamic properties

The study of thermodynamic properties depending on temperature and pressure provides detailed information about material applications and offers a point of view on their fabrication [44].

The thermodynamic parameters such as bulk modulus (B), volume (V), thermal expansion (α), Deybe temperature (θ_D) and heat capacity (C_V) have been calculated using the Gibbs2 package within the quasi-harmonic approach [30]. The temperature-pressure effects on thermodynamic parameters of cubic PbGeO_3 perovskite oxide have been studied in the range of 0 to 1000 K for temperature and 0 to 30 GPa for pressure.

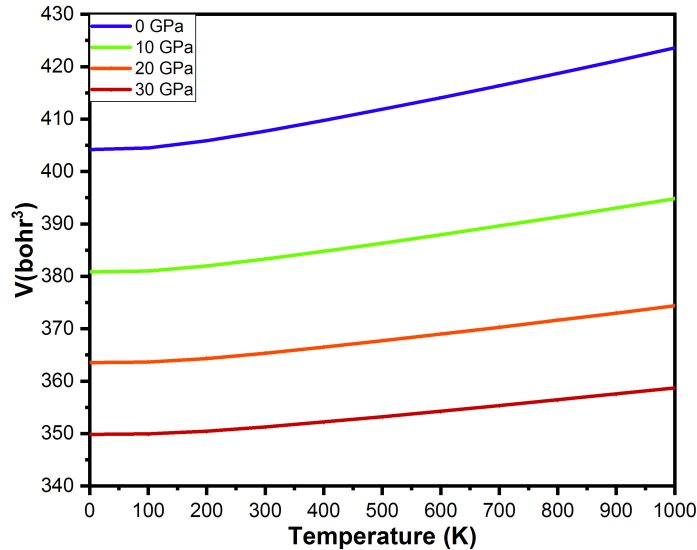


Figure 5: Unit cell volume versus temperature of cubic PbGeO_3 perovskite oxide at different pressures.

The effect of both pressure and temperature on the unit cell volume of cubic $PbGeO_3$ perovskite oxide is illustrated in figure 5. We notice that the volume increases with increasing temperature (expansion), and decreases with increasing pressure (compression). We also remark that the calculated value of volume at 0 GPa and 0 K is in good agreement with what we found in the structural data. The variation of bulk modulus B of $PbGeO_3$ versus temperature at certain pressures is shown in figure 6. We notice that the effect of temperature and pressure on the bulk modulus B is opposite to their effect on the volume curve. Indeed, the bulk modulus B increases with increasing pressure, and it decreases when we increase the temperature. Therefore, the compressibility decreases with pressure at a certain temperature, while it increases with increasing temperature at a particular pressure [45].

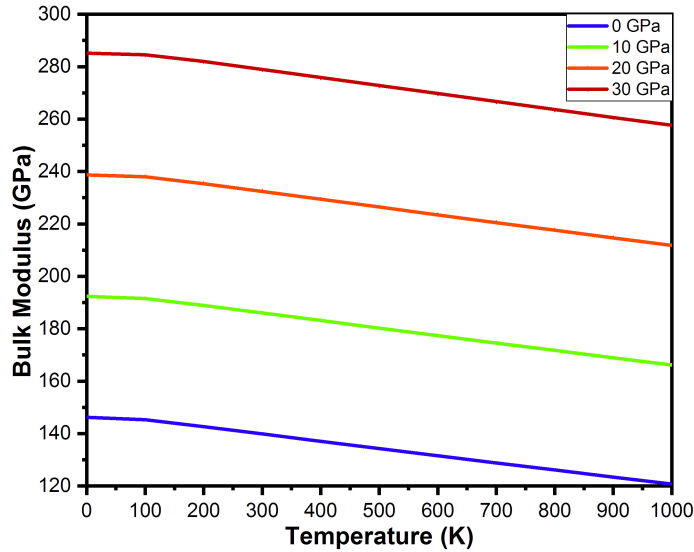


Figure 6: Bulk modulus versus temperature of cubic $PbGeO_3$ perovskite oxide at different pressures.

4.2..1 Thermal expansion

The thermal expansion coefficient (α) of cubic $PbGeO_3$ is calculated with respect to temperature at certain pressures as displayed in figure 7. It is a significant parameter that provides information about the inter-atomic forces of materials, and it is also linked to the anharmonicity of the lattice interaction potential [46].

From figure 7, it can be seen that the expansion coefficient α increases rapidly up to 300 K, then we observe a nearly linear increase at higher temperatures. On the other side, increasing pressure at

a particular temperature leads to a decrease in the thermal expansion coefficient. This result indicates that the $PbGeO_3$ exhibits excellent volume invariance under high pressure [47]. Consequently, increasing pressure and temperature have opposite effects on thermal expansion.

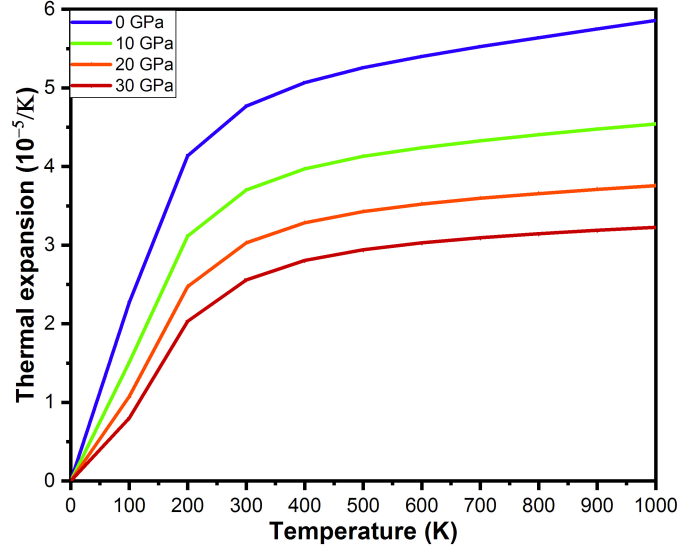


Figure 7: Thermal expansion (α) as a function of temperature of cubic $PbGeO_3$ perovskite oxide at different pressures.

4.2..2 Debye temperatures

The Debye temperature is a special temperature of solids which exhibits the temperature at which the atomic vibrations of material reach their maximum of possible modes [48]. It is a proper estimation of the rigidity of solids [49].

Figure 8 illustrates the Debye temperature versus temperature for $PbGeO_3$ at given pressures. It is obvious that the θ_D curve is approximately constant in the range of 0 to 100 K for all considered values of pressure. This result indicates that the crystal experiences a weak anharmonicity and a slight expansion in this temperature range. Beyond 120 K, the Debye temperature θ_D is reduced gradually with increasing temperature, and this indicates a variation in the atomic vibration spectrum [50].

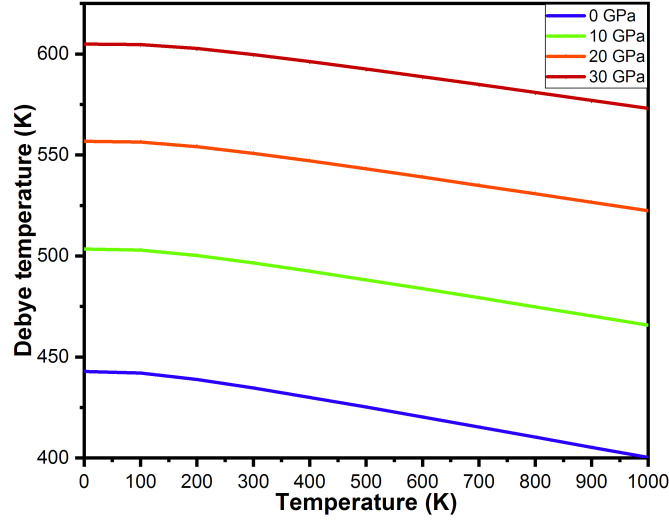


Figure 8: Debye temperature (θ_D) as a function of temperature of cubic $PbGeO_3$ perovskite oxide at different pressures.

4.2.3 Heat capacity

The heat capacity is not only a significant feature that provides the necessary information about the vibrational characteristics of the lattice but also an obligatory parameter for many applications [51]. The variation of the heat capacity C_V of our compound as a function of temperature is shown in figure 9. We notice that the heat capacity presents a similar behavior with different pressures. For a particular pressure, it can be seen that C_V obeys T^3 at low temperatures, which accords with the simple Debye model [52]. Then, the C_V increases slowly with increasing temperature, and it approaches the classical Dulong-Petit limit ($3R \times 5 \text{ atoms} = 15R = 124.71 \text{ J/K.mol}$) at high temperatures. [52].

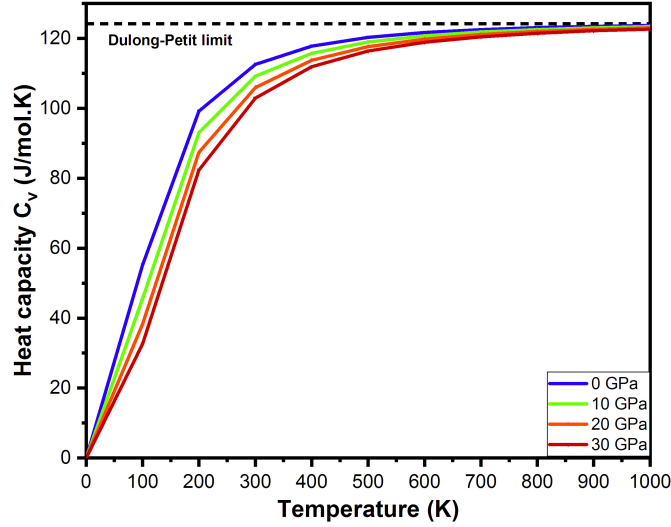


Figure 9: Heat capacity (C_V) with respect to temperature of cubic $PbGeO_3$ perovskite oxide at different pressures.

5. Conclusion

In this paper, we have studied the electronic, elastic, structural, and thermodynamic properties of cubic $PbGeO_3$ based on the FP-LAPW method. The mechanical and elastic parameters are evaluated, and they prove that the cubic $PbGeO_3$ is mechanically stable. In addition, the phonon dispersion shows positive frequencies, confirming that the $PbGeO_3$ compound is dynamically stable. Next, we analyze the electronic properties which reveal that cubic $PbGeO_3$ is a p-type semiconductor with an indirect band gap. Finally, the thermodynamic parameters such as volume, Debye temperature, bulk modulus, and heat capacity are predicted for the cubic $PbGeO_3$ perovskite using quasi-harmonic Debye approximation with pressure and temperature in the range of 0 to 25 GPa and 0 to 1000 K , respectively. Overall, the discussed parameters exhibit the good efficiency of our material.

References

- [1] E.A. Katz, *Helv. Chim. Acta*, DOI:10.1002/hlca.202000061.
- [2] Z. Zeng, Y. Xu, Z. Zhang, Z. Gao, M. Luo, Z. Yin, C. Zhang, J. Xu, B. Huang, F. Luo, Y. Du and C. Yan, *Chem. Soc. Rev.* **49**, 1109-1143 (2020), DOI:10.1039/C9CS00330D.
- [3] M. Kubicek, A.H. Bork and J.L.M. Rupp, *J. Mater. Chem. A*, **5** 11983 (2017), DOI:10.1039/c7ta00987a.
- [4] P. Su, Y. Liu, J. Zhang, C. Chen, B. Yang, C. Zhang and X. Zhao, *J. Phys. Chem. Lett.* **11**, 2812-2817 (2020); DOI:10.1021/acs.jpclett.0c00503.
- [5] M.I. Hussain, R.M.A. Khalil, F. Hussain, M. Imran, A.M. Rana and S. Kim, *Materials Science in Semiconductor Processing* **113** 105064 (2020), DOI:10.1016/j.mssp.2020.105064.
- [6] B. Aïssa, A. Ali and F. El-Mellouhi, *A Contributive Review. Catalysts*, **11**, 1057 (2021), DOI: 10.3390/catal11091057
- [7] A. Muller and T. Kool, *Properties of Perovskites and Other Oxides* (2010), DOI:10.1142/7591
- [8] T. Wolfram and S. Ellialtioglu, *Electronic and Optical Properties of d-band Perovskites* (2006), DOI:10.1017/CB09780511541292
- [9] M. Zhang, G. Liu, D. Zhang, Y. Chen, S. Wen, S. Ruan, *Journal of Alloys and Compounds* **602**, 322–325 (2014), DOI:10.1016/j.jallcom.2014.02.094.
- [10] X. Li, Z. Hu, Y. Cho, X. Li, H. Sun, L. Cong, H.J. Lin, S.C. Liao, C.T. Chen, A. Efimenko, C.J. Sahle, Y. Long, C. Jin, M.C. Downer, J.B. Goodenough and Jianshi Zhou, *Chem. Mater.* **33**, 92-101 (2021), DOI:10.1021/acs.chemmater.0c02706.
- [11] S.C. Sabharwal, S.N. Jha and SANGEETA, *Bull. Mater. Sci.*, Vol. **33**, No. 4 (2010), DOI: 10.1007/s12034-010-0060-6.
- [12] R. Ranjan, D. Pandey and N.P. Lalla, *Phy. Rev. Lett.* **84** (2000), DOI:10.1103/physrevlett.84.3726.
- [13] K. Shahzad , M. Nasir Khan , G. Shabbir and J. Bashir (2011) Neutron and X-Ray Diffraction Crystal Structure Rietveld Analysis of *PbTiO₃* Ceramics, *Ferroelectrics*, **414:1**, 155-161, DOI: 10.1080/00150193.2011.577332.

- [14] R.V. Shpanchenko, V.V. Chernaya, A.A. Tsirlin, P.S. Chizhov, D.E. Sklovsky and E.V. Antipov, Chem. Mater., **16**, 3267-3273 (2004), DOI:10.1021/cm049310x.
- [15] V.G. BHIDE, K.G. DESHMUKH and M.S. HEGDE, Physica **28**, 871-876 (1962), DOI:10.1016/0031-8914(62)90075-7.
- [16] W. Zhou, D. Tan, W. Xiao, M. Song, M. Chen, X. Xiong and J. Xu, J. Phys.: Condens. Matter **24** 435403 (2012), DOI:10.1088/0953-8984/24/43/435403.
- [17] M.P. Moret, M.A.C. Devillers, K. Wörhoff and P. K. Larsen, Journal of Applied Physics **92**, 468 (2002), DOI:10.1063/1.1486048.
- [18] S.S. Subramanian and B. Natesan, Advanced Materials Research Vol. **895** (2014), DOI:10.4028/www.scientific.net/AMR.895.420.
- [19] J.B. Goodenough and J. Zhou, Sci. Technol. Adv. Mater. **16** 036003 (2015), DOI:10.1088/1468-6996/16/3/036003.
- [20] W. Xiao, D. Tan, W. Zhou, M. Chen, X. Xiong, M. Song, J. Liu, H.K. Mao and J. Xu, American Mineralogist, **97**, pages 1193–1198 (2012), DOI:10.2138/am.2012.4021.
- [21] J. Feng, L. Ci, Y. Qi, N. Lun, S. Xiong and Y. Qian, Materials Research Bulletin **57**, 238–242 (2014), DOI:10.1016/j.materresbull.2014.06.011.
- [22] J. Wang, C. Feng, Z. Sun, S. Chou, H.K. Liu and J. Wang, In-situ One-step Hydrothermal Synthesis of a Lead Germanate-Graphene Composite as a Novel Anode Material for Lithium-Ion Batteries (2014), DOI:10.1038/srep07030.
- [23] A. Dey, R. Sharma, S.A. Dar and I.H. Wani, Computational Condensed Matter **26**, e00532 (2021), DOI:10.1016/j.cocom.2020.e00532.
- [24] E.K.U. Gross and R.M. Dreizler, Density Functional Theory (1993), DOI:10.1007/978-1-4757-9975-0.
- [25] P. Blaha, K. Schwarz, F. Tran, R. Laskowski, G.K.H. Madsen and L.D. Marks, J. Chem. Phys. **152**, 074101 (2020), DOI:10.1063/1.5143061.
- [26] J.P. Perdew, K. Burke and M. Ernzerhof, Phys. Rev. Lett. **78**, 1396 (1997), DOI:10.1103/PhysRevLett.77.3865.

- [27] F. Tran and P. Blaha, Phys. Rev. Lett. **102**, 226401 (2009), DOI:10.1103/PhysRevLett.102.226401
- [28] R. Golesorkhtabar, P. Pavone, J. Spitaler, P. Puschnig, C. Draxl, Computer Physics Communications **184**, 1861–1873 (2013), DOI:10.1016/j.cpc.2013.03.010.
- [29] K. Momma and F. Izumi, J. Appl. Cryst. **44**, 1272–1276 (2011), DOI:10.1107/S0021889811038970.
- [30] A.O. Roza, D.A. Pérez and V. Luaña, Computer Physics Communications **182**, 2232–2248 (2011), DOI:10.1016/j.cpc.2011.05.009.
- [31] M.A. Blanco, E. Francisco, V. Luaña, Computer Physics Communications **158**, 57–72 (2004), DOI:10.1016/j.comphy.2003.12.001.
- [32] A. Togo, I. Tanaka, Scripta Materialia 108 1–5 (2015), 10.1016/j.scriptamat.2015.07.021.
- [33] H. Mizoguchi, T. Kamiya, S. Matsuishi and H. Hosono, Nat. Commun. **2**, 470 (2011), DOI:10.1038/ncomms1484.
- [34] N. Pandech, K. Sarasamak and S. Limpijumnong, Journal of Applied Physics **117**, 174108 (2015), DOI:10.1063/1.4919837.
- [35] F. Mouhat and F.X. Coudert, PHYSICAL REVIEW B **90**, 224104 (2014), DOI:10.1103/PhysRevB.90.224104.
- [36] A. Bouhemadou, D. Allali, K. Boudiaf, B. Al Qarni, S. Bin-Omran, R. Khenata and Y. Al-Douri, Electronic, optical, elastic, thermoelectric and thermodynamic properties of the spinel oxides $ZnRh_2O_4$ and $CdRh_2O_4$, Journal of Alloys and Compounds (2018), DOI:10.1016/j.jallcom.2018.09.338.
- [37] A.M. Shawahni, M.S. Abu-Jafar, R.T. Jaradat, T. Ouahrani, R. Khenata, A.A. Mousa and K.F. Ilaiwi, Materials, **11**, 2057 (2018), DOI:10.3390/ma11102057.
- [38] R. Ali, G. Murtaza, Y. Takagiwa, R. Khenata, H. Uddin, H.Ullah and S.A. Khan, CHIN. PHYS. LETT. Vol. **31**, 047102 (2014), DOI:10.1088/0256-307X/31/4/047102
- [39] S.A. Dar, R. Sharma, V. Srivastava and U.K. Sakalle, RSC Adv., **9**, 9522 (2019), DOI:10.1039/c9ra00313d.

- [40] V. Tvergaard, J.W. Hutchinson, J. Am. Ceram. SOC, **71**, 157-66 (1988), DOI:10.1111/j.1151-2916.1988.tb05022.x.
- [41] U.Qazi, S. Mehmood, Z. Ali, I. Khan, I. Ahmad, Physica B **624**, 413361 (2022), DOI:10.1016/j.physb.2021.413361.
- [42] M. Hasan, S. Nasrin, M.N. Islam and A.K.M.A. Hossain, AIP Advances **12**, 085327 (2022); DOI:10.1063/5.0104191.
- [43] S.A. Dar, V. Srivastava and U.K. Sakalle, Journal of Magnetism and Magnetic Materials **484** 298–306 (2019), DOI:10.1016/j.jmmm.2019.04.048.
- [44] L. Qiang, H.D. Hui, C.Q. Long and W.F Hou, Chin. Phys. B **22**, 037101 (2013), DOI:10.1088/1674-1056/22/3/037101.
- [45] Jin, Z., Wu, Y., Li, S., Wu, Q., Chen, S., Chen, Y., Zhang, W., Zhang, C., Electronic Structure, Elastic, Optical and Thermodynamic Properties of Cubic Perovskite $NaBaF_3$ with Pressure Effects: First-principles Calculations, Results in Physics (2021), DOI:10.1016/j.rinp.2021.103860
- [46] S.A. Dar, V. Srivastava, U.K. Sakalle and V. Parey, Eur. Phys. J. Plus **133**, 64 (2018), DOI: 10.1140/epjp/i2018-11889-y.
- [47] L.A. Irtyugo, L.T. Denisova, V.M. Denisov, N.V. Belousova and A.S. Samoilov, Journal of Siberian Federal University. Chemistry **1** 37-40 (2012).
- [48] J.D. Zhang, X.L. Cheng and D.H Li, Journal of Alloys and Compounds 9577-9582 **509**, (2011), DOI:10.1016/j.jallcom.2011.07.093.
- [49] M. Ziaty and H. Ez-Zahraouy, J Phy Opt Sci **3**, 1-8 (2021).
- [50] I. Hattabi, A. Abdiche, S.H. Naqib and R. Khenata, Chinese Journal of Physics **59**, 449–464 (2019), DOI:10.1016/j.cjph.2019.04.011.
- [51] O. NEMIRI, S. GHEMID, Z. CHOUAHDA, H. MERADJI and F. EL HAJ HASSAN, International Journal of Modern Physics B **27**, 1350166 (2013), DOI:10.1142/S021797921350166X.
- [52] S. Wang, M. Mohammadi, I. Dirba, K. Hofmann, B. Albert, L. Alff, P. Komissinskiy and L. Molina-Luna, Computational Materials Science **197**, 110609 (2021), DOI:10.1016/j.commatsci.2021.110609.